1-1-2005

Liquid-crystal imaging of molecular-tilt ordering in self-assembled lipid tubules

Yue Zhao
University of Central Florida

Nidhi Mahajan
University of Central Florida

Ruibo Lu
University of Central Florida

Jiyu Fang
University of Central Florida

Liquid-crystal imaging of molecular-tilt ordering in self-assembled lipid tubules

Yue Zhao, Nidhi Mahajan, Ruibo Lu, and Jiyu Fang*

Advanced Materials Processing and Analysis Center, Department of Mechanical, Materials, and Aerospace Engineering, University of Central Florida, Orlando, FL 32816

Edited by H. Eugene Stanley, Boston University, Boston, MA, and approved April 6, 2005 (received for review December 15, 2004)

Self-assembled cylindrical tubules of chiral phospholipids are interesting supramolecular structures. Understanding the molecular-tilt order is a key step in controlling the size and shape of the tubules and designing new functional materials. The current theories based on the chiral interactions, coupled with molecular tilt, have predicted that the tubules could have both uniform and modulated tilt states. Here, we image the molecular-tilt order in the self-assembled tubules of a chiral phospholipid by using liquid crystals as an optical amplification probe. We demonstrate that the organization of the molecular-tilt azimuth in the lipid tubules can induce an azimuthal orientation in the liquid crystals. Both uniform and modulated tilt states of the lipid tubules are observed after liquid-crystal optical amplification.

liquid-crystal amplification | molecular ordering | self-assembly | optical amplification | supramolecular structure

The self-assembled cylindrical tubules have attracted considerable attention because of their interesting supramolecular structures and technological applications (1, 2). It has been found that a variety of amphiphilies, including alkylaldonamides (3), diacetylenic phospholipids (4, 5), amino acid-based surfactants (6, 7), and multicomponent mixtures in bile (8, 9), self-assemble into cylindrical tubules in solutions. Recently, advances have been made in controlling the sizes and shapes of tubules by adjusting the chemical compositions and the conditions under which self-assembly occurs (10–16).

Theoretical models based on the chiral interactions, coupled with molecular tilt, have been used to explain the formation of the cylindrical tubules (17–19). In these models, the chiral molecules do not pack parallel to their neighbors but, rather, at a nonzero angle with respect to their neighbors. This chiral packing causes the twisting of a bilayer stripe, which leads to the formation of cylindrical tubules. The model by Selinger *et al.* (19) suggests that the tubules can have both uniform and modulated tilt states. In the uniform tilt state, the tubule has a constant orientation of the molecule tilt with respect to the equator of the cylinder (Fig. 1*a*). In the modulated tilt state, the tubule has a periodic modulated structure by helical stripes in the molecular tilted direction winding around the cylinder. The direction of the molecular tilt smoothly varies across the stripes and jumps at the edges of the stripes (Fig. 1*b*). These stripes in the tubules are suggested to be analogous to the tilted stripes seen in the Langmuir monolayers (20) but in a cylindrical rather than a planar geometry. To our knowledge, there has been no experimental test of the theoretical predictions because of the difficulty in probing the local direction of the molecular tilt in the tubules.

In recent years, there has been an increased interest in developing an imaging technique based on liquid-crystal optical amplification for studying the structures and physical properties of organic and biological interfaces (21–25). It has been demonstrated that liquid crystals can map differences in the spatial orientation of terminal groups in self-assembled monolayers (SAMs) formed from alkanethiols that differ by single methylene (21). This change in the spatial orientation between odd and even number of methylene groups in SAMs can cause a 90° rotation in the azimuthal direction of liquid crystals. In ref. 22, we showed that the variation of the molecular tilt direction in the Langmuir monolayer of 1-monopalmitoyl-*rac*-glycerol can induce an azimuthal orientation in nematic liquid-crystal layers. After the liquid-crystal optical amplification, the tilted textures in the monolayer can be easily visualized with a polarizing optical microscope. In this study, we imaged the molecular-tilt ordering in the self-assembled tubules of a chiral phospholipid by using liquid crystals as an optical amplification probe. We observed both uniform and modulated tilt states of the lipid tubules, which have been predicted by current theories.

Materials and Methods

Lipid tubules were prepared by controlling the cooling process of a 5 mg/ml suspension of 1,2-bis(tricosa-10,12-diynoyl)-sn-glycero-3-phosphocholine ($DC_{8,9}PC$) (Avanti Polar Lipids) in ethanol/water (70:30, vol/vol). The polymerization of the tubule suspension was performed with the UV irradiation (254 nm) for 20 min at room temperature. A drop of a tubule solution was placed and then dried on octadecyltrichlorosilane monolayer coated glass slides, which generate homeotropic alignment of liquid crystals. Sealed cells containing 4-pentyl-4′-cyanolbiphenyl (5CB) (BDH) or MLC-6609 (EM Laboratories, Elmsford, NY) liquid crystals were prepared with two glass slides. The $DC_{8,9}PC$ tubules were deposited on one of them. The two glass slides were separated by a 25-μm Mylar spacer. Liquid-crystal orientation in the cells was examined by using a polarizing optical microscope (BX 40, Olympus), and images were captured by using a digital camera (C2020 Zoom, Olympus) mounted on the microscope. Image analysis was preformed with MATLAB software. For the polarizing microscope, the optics was adjusted to complete extinction before placing samples on the stage. An atomic force microscope (Dimension 3100, Digital Instruments, Santa Barbara, CA) was used to study the structure of the lipid tubules deposited on glass substrates. Silicon nitride cantilevers (Nanosensors, Neuchatel, Switzerland) with a resonant frequency of ≈260 kHz were used. The cantilever was excited just below its resonant frequency. All atomic force microscope (AFM) measurements were performed in the tapping mode at a scan rate of 0.5 Hz in air at room temperature.

Results and Discussion

Fig. 1*c* is an AFM image of a lipid tubule immobilized on a glass substrate. This AFM image was taken 6 h after the tubule was dried in air at room temperature. The tubule shows a slightly flattened top surface with an end of the twisted bilayer stripe, suggesting that it is formed by rolled up of bilayer stripes. Thomas *et al.* (26) directly observed the tubule formation in the early stage with optical microscopy and found that, as the gaps between the bilayer stripes closed, the helical ribbon turned to

This paper was submitted directly (Track II) to the PNAS office.

Abbreviations: 5CB, 4-pentyl-4′-cyanolbiphenyl; AFM, atomic force microscope; $DC_{8,9}PC$, 1,2-bis(tricosa-10,12-diynoyl)-sn-glycero-3-phosphochloline.

*To whom correspondence should be addressed. Email: jfang@mail.ucf.edu.

www.pnas.org/cgi/doi/10.1073/pnas.0409366102

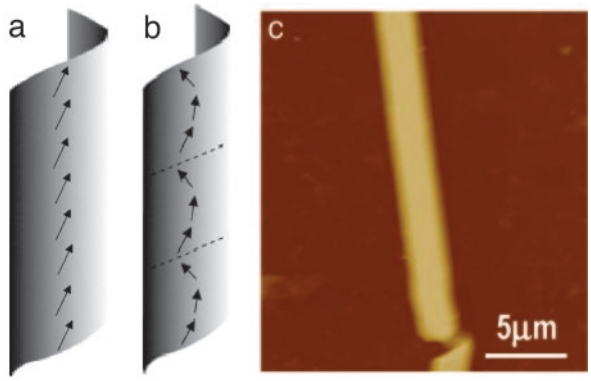

Fig. 1. Predicted tilt states of lipid tubules. (*a* and *b*) Schematic representations of self-assembled lipid tubules with the uniform (*a*) and modulated (*b*) tilt direction. (*c*) AFM image of a lipid tubule immobilized on a glass substrate. The molecular azimuth direction is indicated by the arrows in *a* and *b*.

a cylindrical tubule. It is clear from Fig. 1*c* that the edges of the bilayer stripes fuse to form a continuous homogeneous tubule. There are no seams observed on the tubule surface. The flattening is believed to a result of the drying on the glass substrate. The cross section measurement shows that the tubule is ≈0.696 μm in height, which agrees with the diameter of single tubules. The apparent width of the tubule in the AFM image is 3.2 μm. The increased width is attributed to the geometrical effects of the AFM tip and the drying process.

Fig. 2 shows liquid-crystal 5CB images of a lipid tubule between crossed polarizer and analyzer. Here, the optical contrast is a result of the orientation changes of the liquid-crystal 5CB. We found that the tubule is lighted up by the 5CB, and it changes its brightness upon rotation of the sample. The tubule becomes dark and disappears in the liquid-crystal image if the direction of its axis is 45° to the polarizer (Fig. 2 *a* and *c*), and it becomes bright if the direction is parallel to the polarizer (Fig. 2 *b* and *d*). We carefully measured the intensity of the transmitted light through a number of the tubules during their rotation to quantify the uniformity of azimuthal orientation of the 5CB with the image analysis. A strong modulation in the intensity of the transmitted light was observed (Fig. 2*e*). The tubules show the maximum transmittance when they are parallel to the polarizer and the minimum transmittance when they are orientated by 45° with respect to the polarizer. These measurements led us to conclude that the lipid tubules induce uniform azimuthal orientation of the 5CB in a direction that is ≈45° to the tubule axis. To understand the interactions that drive the azimuthal orientation of the liquid crystal, we tested the orientation of the MLC-6609 on the lipid tubules. It was found that the MLC-6609 also showed a uniform azimuthal direction, which is ≈45° to the tubule axis. Because the anisotropy of the dielectric constant is positive ($\Delta\varepsilon = +8$) for 5CB but negative for MLC 6609 ($\Delta\varepsilon = -4.2$), it is likely that the coupling between the liquid-crystal molecules and lipid tubules that gives to the preferred azimuthal direction is not due to the dielectric coupling of the liquid crystal to the electric field of tubule surface. X-ray diffraction (27) has revealed that the lipid molecules are tilted with respect to the normal of the tubule surface. Here, the first layer of the 5CB molecules might partially penetrate into the tilted lipid bilayer to adopt the lipid orientation through the chain–chain interaction. The long-range orientation correlation of the liquid crystal leads to the surface-induced tilt order into the bulk phase. The penetration of the 5CB molecules in lipid monolayers has been reported (28–30). These studies also show that the 5CB adopt the orientation of the lipid molecules to form a uniformly aligned liquid-crystal layer on the lipid monolayers.

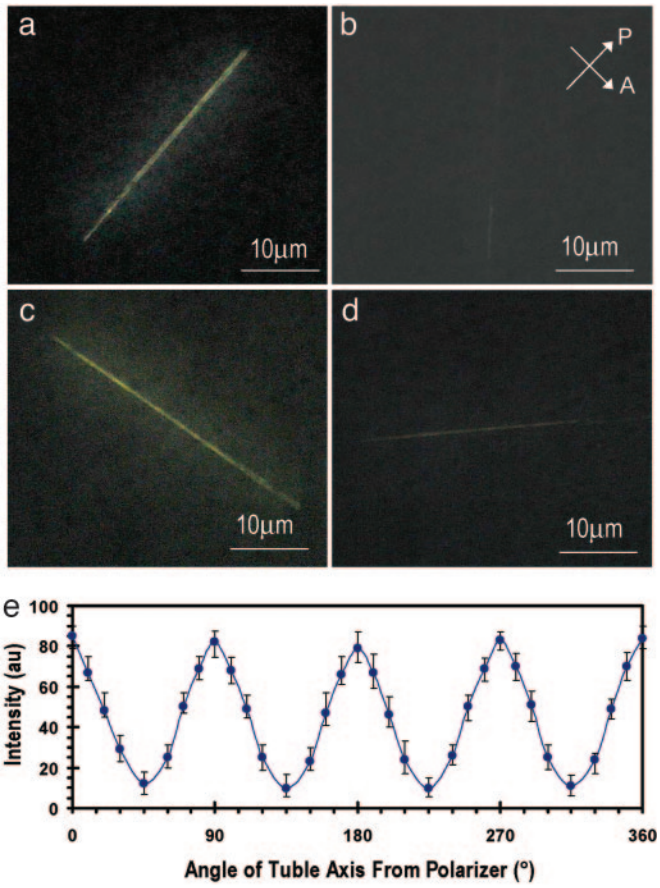

Fig. 2. Liquid-crystal images of uniform tilt state. (*a–d*) Polarizing microscope images of a lipid tubule below the nematic liquid-crystal 5CB. Images were taken when the tubule was rotated between crossed polarizer (P) and analyzer (A). Arrows indicate the directions of polarizer and analyzer. (e) Plots of the intensity of the transmitted light through the 5CB anchored on the surface of the tubules as function of the angle between the direction of the tubule and the analyzer. The measurements of the intensity on six different tubules were performed by image analysis with MATLAB software.

We conclude that the preferred azimuthal direction of the 5CB shown in Fig. 2 reflects the uniform tilt state of the lipid tubules.

Not all lipid tubules below the 5CB show uniform brightness when they are viewed with a polarizing microscope. For example, we found that a featureless tubule in the unpolarizing optical microscopy (Fig. 3*a*) shows birefringence helical stripes in the polarizing optical microscopy (Fig. 3*b*). These birefringence stripes are a result of the orientation changes of the liquid-crystal 5CB on the tubule surface. They are lost when the 5CB is heated into the isotropic phase but reappear when the 5CB is cooled down to the nematic phase, which is clear evidence that the birefringence helical stripes in the liquid-crystal image are induced by the tubule. Fig. 3*c* is a liquid-crystal image of multiple lipid tubules between crossed polarizer and analyzer. The birefringence helical stripes are observed on three tubules, which are orientated at slightly different directions. We carefully measured the intensity of the transmitted light across the width of the birefringence helical stripes with the image analysis. We found that the intensity has a minimum at both edges of the stripes and reaches a maximum in the middle of the stripes (Fig. 3*d*). The changes of the transmitted intensity reflect the variations of the tilt azimuth direction of the 5CB across the width of the birefringence stripes. We conclude that the observed birefringence helical stripes reflect the modulated tilt state of the lipid

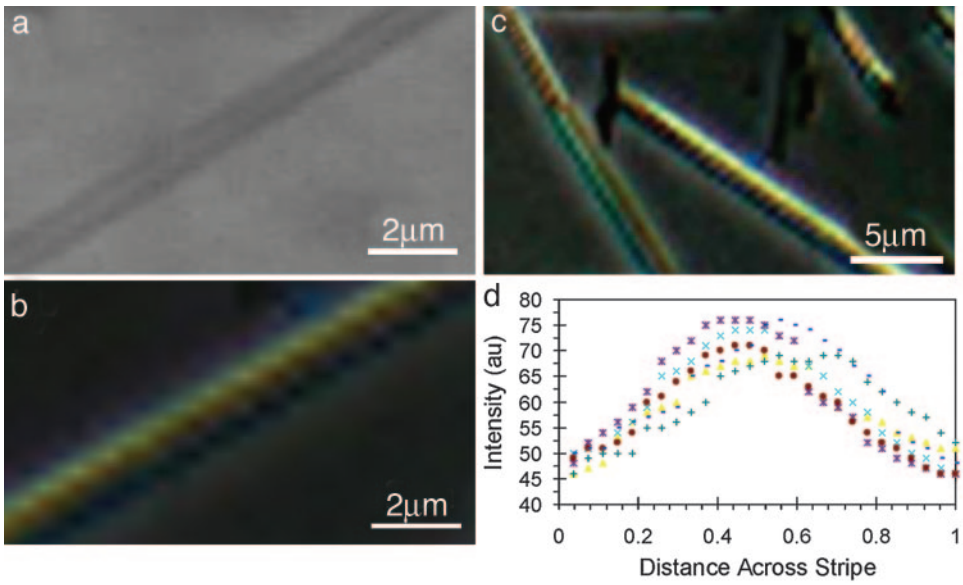

Fig. 3. Liquid-crystal images of modulated tilt state. (*a* and *b*) Nonpolarizing (*a*) and polarizing (*b*) microscope images of a lipid tubule below the nematic liquid-crystal 5CB. (*c*) Polarizing microscope image of multiple lipid tubules below the 5CB. (*d*) Plots of the intensity of the transmitted light as a function of the fractional distance across the width of the helical stripes. The measurements of the intensity were performed by image analysis with MATLAB software.

tubules. Based on statistic analysis of the liquid-crystal images of the tubules, we found that ≈10% of the lipid tubules show the modulated tile state.

To further understand the director distributions of the liquid-crystal 5CB on the lipid microtubule, we used a finite-element method (31), which is known as a useful three-dimensional modeling for a complicated structure with an arbitrary geometry, to explain the liquid-crystal images of the lipid tubules. It is known that the optical properties of liquid crystals are determined by the director, which represents the local orientation of the molecules. By giving the boundary conditions, the director in the interior of the liquid crystal can be calculated by minimizing the total free energy, which is the summation of the elastic free energy and the surface free energy as follows:

$$f_g = f_e + f_s, \qquad [1]$$

where f_g, f_e, and f_s are the total free energy, the elastic free energy, and the surface free energy, respectively.

The total free energy in the direction of the director vector can be written as follows:

$$[f_g]_{n_i} = \frac{\partial f_g}{\partial_{n_i}} - \frac{d}{dx}\left[\frac{\partial f_g}{\partial(dn_i/dx)}\right] - \frac{d}{dyf}\left[\frac{\partial f_g}{\partial(dn_i/dy)}\right] - \frac{d}{dz}\left[\frac{\partial f_g}{\partial(dn_i/dz)}\right]. \qquad [2]$$

By substituting Eq. **2** to Eq. **1**, after simplification the separated form of the total free energy is related to the elastic free energy and the surface free energy as follows (32):

$$[f_g]_{n_i} = [f_e]_{n_i} + [f_s]_n. \qquad [3]$$

The elastic free energy f_e is calculated from the following Oseen–Frank free-energy equation (33):

$$f_e = \frac{1}{2}K_{11}(\nabla\cdot\hat{n})^2 + \frac{1}{2}K_{22}(\hat{n}\cdot\nabla \times \hat{n} + q_0)^2 + \frac{1}{2}K_{33}|(\hat{n}\times\nabla\times\hat{n})|^2, \qquad [4]$$

where q_0 is the inherent chiral term; $\hat{n}$ is the director vector; and K_{11}, K_{22}, and K_{33} are the splay, twist, and bend elastic constant, respectively.

The potential distribution can be solved as a variational problem with a finite-element method, where the liquid-crystal cell is discretized with the first-order hexahedral element and the periodic boundary condition is applied in the (x, y) plane. Strong anchoring is assumed to the liquid-crystal director and the Dirichlet boundary condition is imposed on the resultant matrix equations. The normalized light transmittance through the liquid-crystal medium under the crossed polarizers can be described as follows (34):

$$T/T_o = \sin^2(2\varphi)\sin^2[\pi d\cdot\Delta n/\lambda], \qquad [5]$$

where φ is the rotation angle of liquid-crystal director, Δn is the liquid-crystal birefringence, d is the cell gap, and λ is the wavelength of the incident light.

For the liquid-crystal 5CB at room temperature, we have $\lambda = 0.5\ \mu$m and $\Delta n = 0.18$. During the simulation process, we assumed that the liquid crystal is aligned on the bilayer walls of the lipid microtubules. Therefore, in the region where the bilayers are located, there would be the extra phase retardation between the neighboring liquid-crystal medium. The effective birefringence can be described as follows (35):

$$\Delta n_{eff}(\theta, \varphi) = \frac{n_o n_e}{\sqrt{n_o^2\sin^2\theta + n_e^2\cos^2\theta}} - n_o \neq \Delta n. \qquad [6]$$

Here, θ is the tile angle of liquid-crystal molecules on the bilayers, and n_e and n_o are the extraordinary and ordinary index of liquid-crystal molecules, respectively.

We modeled the lipid tubule by a cylinder with a slightly flattened top surface extended along the *y* axis. The 5CB on the tubules is assumed to be tilted by 45° from the local surface normal (Fig. 4*a*). The azimuthal direction of the 5CB gradually changes on the tubule surface (Fig. 4*b*). Along the glass slide, the anchoring is homeotropic (i.e., the director points perpendicular to the surface). When we have derived the director configuration shown in Fig. 4 *a* and *b*, we calculate the transmitted intensity profile around the microtubule. Fig. 4*c* shows the resulted

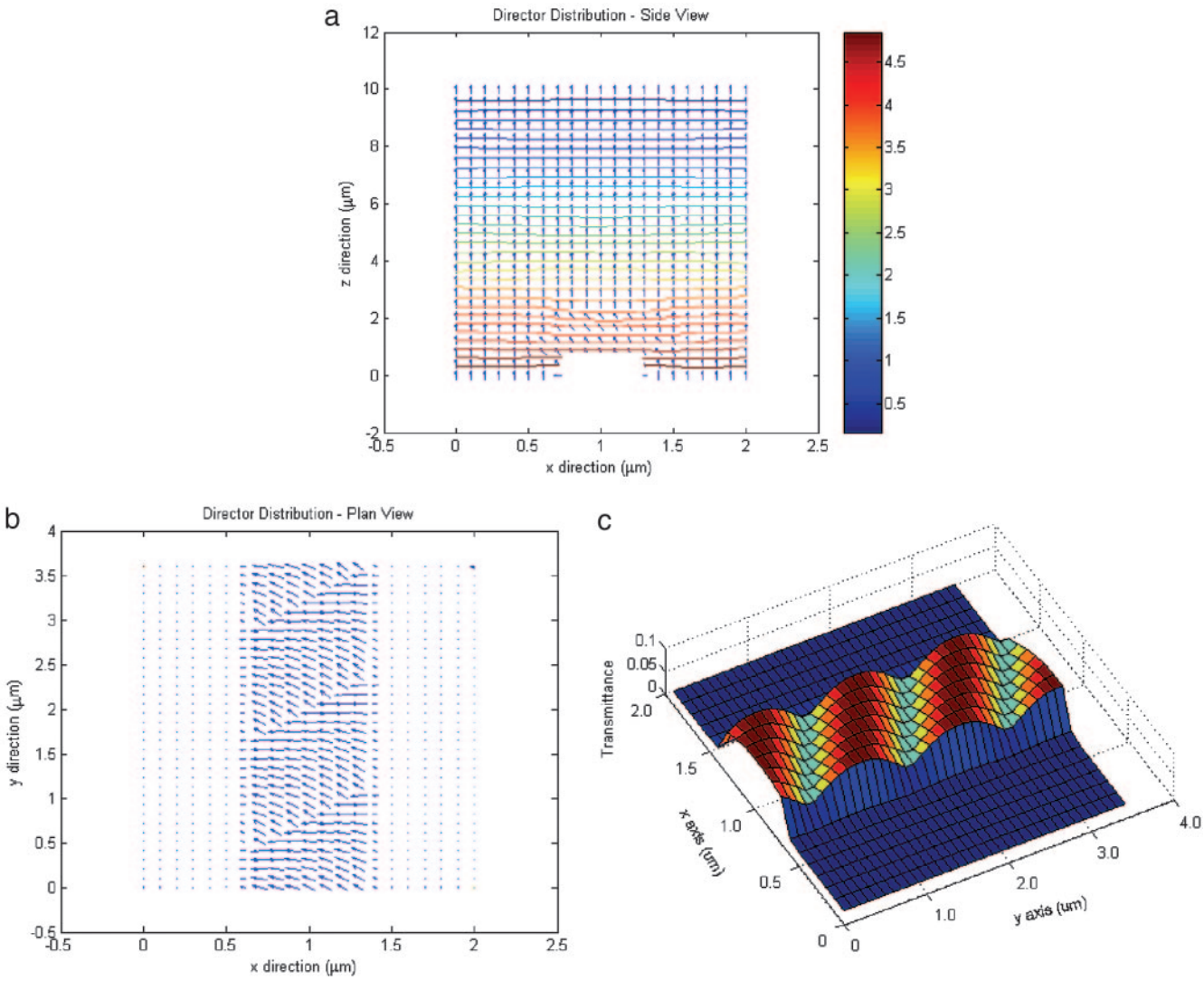

Fig. 4. Modeling of liquid-crystal director. (*a* and *b*) Minimum-energy configuration for the liquid-crystal director above a lipid tubule in the *xz* (*a*) and *xy* (*b*) planes. (*c*) Corresponding profile of the transmitted intensity in the *xy* plane.

pattern of the transmitted intensity profile around the tubule. The theoretic image also shows birefringence helical stripes, which are comparable with the experimental image shown in Fig. 3*b*. This consistency suggests that our assumption for the anchoring of the 5CB on the tubule surface is appropriate.

Although we have not fully understood the origin of the molecular-level interaction between the 5CB and the $DC_{8,9}PC$ that leads to the azimuthal orientation in the liquid-crystal layer, it is likely that the 5CB molecules in the first layer partially penetrate into the tilted lipid bilayer to adopt the lipid orientation through the chain–chain interaction. The surface-induced tilt order is extended into the bulk phase because of the long-range orientation correlation of the liquid crystal. The liquid-crystal optical amplification allows us to visualize the molecular tilt states in the lipid tubules with a polarizing optical microscope. Our results demonstrate that the self-assembled tubules of the $DC_{8,9}PC$ have both uniform and modulated tilt states. An understanding of the molecular tilt orientation is a key step in controlling the size and shape of lipid tubules and designing new structures for nanotechnology.

This work was supported by University of Central Florida's nanoinitiative. We thank one of the reviewers of this manuscript in the early version for suggestions that resulted in the experimental data given in this article and helped us clarify some issues presented in this work.

1. Fuhrhop, J. H. & Helfrich, W. (1993) *Chem. Rev.* **93,** 1565–1582.
2. Schnur, J. M. (1993) *Science* **262,** 1669–1676.
3. Fuhrhop, J. H., Schnieder, P., Boekema, E. & Helfrich, W. (1988) *J. Am. Chem. Soc.* **110,** 2861–2867.
4. Georger, J. H., Singh, A., Price, R. R., Schnur, J. M. Yager, P. & Schoen, P. E. (1987) *J. Am. Chem. Soc.* **109,** 6169–6175.
5. Thomas, B. N., Corcoran, R. C., Cotant, C. L., Lindemann, C. M., Kirsch, J. E. & Persichini, P. J. (1998) *J. Am. Chem. Soc.* **120,** 12178–12186.
6. Imae, T., Takahashi, Y. & Muramatsu, H. (1992) *J. Am. Chem. Soc.* **114,** 3414–3419.
7. Oda, R., Huc, I., Schmutz, M., Candau, S. J. & MacKintosh, F. C. (1999) *Nature* **399,** 566–569.
8. Chung, D. S., Benedek, G. B., Konikoff, F. M. & Donovan, J. M. (1993) *Proc. Natl. Acad. Sci. USA* **90,** 11341–11345.
9. Zastavker, Y. V., Asherie, N., Lomakin, A., Pande, J., Donovan, J. M., Schnur, J. M. & Benedek, G. B. (1999) *Proc. Natl. Acad. Sci. USA.* **96,** 7883–7887.
10. Thomas, B. N., Safinya, C. R., Plano, R. J. & Clark, N. A. (1994) *Science* **267,** 1635–1638.
11. Spector, M. S., Singh, A., Messersmith, P. B. & Schnur, J. M. (2001) *Nano. Lett.* **1,** 375–378.

12. Song, J., Cheng, Q., Kopta, S. & Stevens, R. C. (2001) *J. Am. Chem. Soc.* **123,** 3205–3213.
13. John, G., Jung, J. H., Minamikawa, H., Yoshida, K. & Shimizu, T. (2002) *Chem. Eur. J.* **8,** 5494–5500.
14. Singh, A., Wong, E. M. & Schnur, J. M. (2003) *Langmuir* **19,** 1888–1898.
15. Pakhomov, S., Hammer, R. P., Mishra, B. K. & Thomas, B. N. (2003) *Proc. Natl. Acad. Sci. USA* **90,** 11341–11345.
16. Lee, S. B., Koepsel, R., Stolz, D. B., Warriner, H. E. & Russell, A. (2004) *J. Am. Chem. Soc.* **126,** 13400–13405.
17. Helfrich, W. & Prost, J. (1988) *Phys. Rev. A* **38,** 3065–3068.
18. Ou-Yang, Z. C. & Liu, J. X. (1991) *Phys. Rev. A* **43,** 6826–6836.
19. Selinger, J. V., Spector, M. S. & Schnur, J. M. (2001) *J. Phys. Chem. B* **105,** 7157–7169.
20. Ruiz-Garcia, J., Qiu, X., Tsao, M. W., Marshall, G., Knobler, C. M., Overbeck, G. A. & Mobius, D. (1993) *J. Phys. Chem.* **97,** 6955–6957.
21. Gupta, V. K. & Abbott, N. L. (1996) *Phys. Rev. E* **54,** 4540–4543.
22. Fang, J. Y., Gehlert, U., Shashidar, R. & Knobler, C. M. (1999) *Langmuir* **15,** 297–299.
23. Gupta, V. K., Skaife, J. J., Dubrovsky, T. B. & Abbott, N. L. (1998) *Science* **279,** 2077–2080.
24. Cheng, Y. L., Batchelder, D. N., Evans, S. D., Henderson, J. R., Lydon, J. E. & Ogier, S. D. (2000) *Liquid Crystals* **27,** 1267–1275.
25. Fang, J. Y., Ma, W., Selinger, J. V. & Shashidhar, R. (2003) *Langmuir* **19,** 2865–2869.
26. Thomas, B. N., Lindemann, C. M. & Clark, N. A. (1999) *Phys. Rev. E* **59,** 3040–3047.
27. Caffrey, M., Hogan, J. & Rudolph, A. S. (1991) *Biochemistry* **30,** 2134–2146.
28. Huang, J. Y., Superfine, R. & Shen, Y. R. (1990) *Phys. Rev. A* **42,** 3660–3663.
29. Hiltrop, K., Haase, J. & Stegemeyer, H. (1994) *Ber. Bunsenges. Phys. Chem.* **98,** 209–216.
30. Kühnau, U., Petrov, A. G., Klose, G. & Schmiedel, H. (1999) *Phys. Rev. E* **59,** 578–585.
31. Dhatt, G. & Touzoy, G. (1984) *The Finite Element Method Displayed* (Thomson, New Delhi).
32. Anderson, J. E., Watson, P. E. & Bos, P. J. (1993) *LC3D: Liquid Crystal Display 3-D Director Simulator Software and Technology Guide* (Artech House, Boston).
33. Gennes, P. G. de & Prost, J. (1993) *The Physics of Liquid Crystals* (Oxford Univ. Press, New York).
34. Lien, A. (1997) *Liquid Crystal* **22,** 171–175.
35. Lueder, E. (2001) *Liquid Crystal Displays: Addressing Schemes and Electro-optic Effects* (Wiley, New York).